Original Article

JCBFM

Journal of Cerebral Blood Flow & Metabolism
2021, Vol. 41(4) 901–913

DOI: 10.1177/0271678X20935274
journals.sagepub.com/home/jcbfm
SAGE

Altered coupling of cerebral blood flow and functional connectivity strength in visual and higher order cognitive cortices in primary open angle glaucoma

Qian Wang[1,*], Xiaoxia Qu[1,*], Weiwei Chen[2], Huaizhou Wang[2], Caiyun Huang[1], Ting Li[1], Ningli Wang[2] and Junfang Xian[1]

Abstract

Primary open-angle glaucoma (POAG) has been suggested to be a neurodegenerative disease associated with altered cerebral vascular hemodynamics and widespread disruption of neuronal activity within the visual, working memory, attention and executive networks. We hypothesized that disturbed neurovascular coupling in visual and higher order cognitive cortices exists in POAG patients and correlates with glaucoma stage and visual field defects. Through multimodal magnetic resonance imaging, we evaluated the cerebral blood flow (CBF)-functional connectivity strength (FCS) correlations of the whole gray matter and CBF/FCS ratio per voxel for all subjects. Compared with normal controls, POAG patients showed reduced global CBF-FCS coupling and altered CBF/FCS ratios, predominantly in regions in the visual cortex, salience network, default mode network, and dorsal attentional network. The CBF/FCS ratio was negatively correlated with glaucoma stage, and positively correlated with visual field defects in the lingual gyrus in POAG patients. Moreover, early brain changes were detected in early POAG. These findings indicate neurovascular coupling dysfunction might exist in the visual and higher order cognitive cortices in POAG patients and its clinical relevance. The results may contribute to the monitoring of POAG progression and provide insight into the pathophysiology of the neurodegenerative process in POAG.

Keywords

Cerebral blood flow, functional connectivity, neurovascular coupling, primary open-angle glaucoma, resting state

Received 8 January 2020; Revised 8 May 2020; Accepted 26 May 2020

Introduction

Glaucoma is the most frequent cause of irreversible blindness worldwide.[1] Primary open-angle glaucoma (POAG) is six times more common than primary angle-closure glaucoma.[2] Currently, intraocular pressure (IOP) is the only modifiable risk factor for POAG, although the loss of retinal ganglion cells and visual defects can continue despite well-controlled IOP. The major drawback of current methods for POAG diagnosis is that the disease is not diagnosable until considerable damage to the retina has already occurred, which has led to extensive efforts to identify a novel method for early POAG diagnosis.

Experimental evidence supports the notion that POAG is a widespread neurodegenerative condition

[1]Department of Radiology, Beijing Tongren Hospital, Capital Medical University, Beijing, China
[2]Beijing Institute of Ophthalmology, Beijing Tongren Eye Center, Beijing Tongren Hospital, Capital Medical University

*These authors contributed equally to this work and should be regarded as equivalent first authors.

Corresponding authors:
Junfang Xian, Department of Radiology, Beijing Tongren Hospital, Capital Medical University, Beijing, No.1 of Dongjiaominxiang Street, Dongcheng District, Beijing 100730, China.
Email: cjr.xianjunfang@vip.163.com

Ningli Wang, Beijing Tongren Eye Center, Beijing Tongren Hospital, Capital Medical University, Beijing Ophthalmology and Visual Sciences Key Laboratory, No.1 Dongjiaominxiang Street, Dongcheng District, Beijing 100730, China.

associated with the central nervous system (CNS).[3–6] In addition, close links between POAG and Alzheimer's disease (AD) have been observed.[7] Studies have established deposition of amyloid β (Aβ) and tau in the retina and vitreous of glaucoma patients, consistent with the pattern found in the cerebral spinal fluid of patients with AD.[8,9] Impaired neurovascular coupling has been suggested as the earliest pathological event in AD, which might serve as an early biomarker of cerebral pathology.[10] Similarly, neurovascular coupling dysfunction in the optic nerve head plays a pivotal role in glaucomatous optic neuropathy.[11,12] Furthermore, studies have demonstrated that the glaucomatous loss of retinal ganglion cells and their axons are accompanied by changes in astrocytes and retinal microglial cells.[13,14] Astrocyte glial cells are one of the major components of neurovascular coupling.[15] The malfunction of these cells in glaucoma may not only lead to the death of retinal ganglion cells but also be accompanied or preceded by disruption in neurovascular coupling.[11,16–18]

The retina is a 'window' into the brain, and diseases behave the same in the CNS as they do in the retina.[19] Studies in humans and other primates have shown that glaucomatous damage spreads beyond the eye and the optic nerve. Widespread damage to gray matter, anatomic connectivity and functional connectivity can go beyond the visual system in patients with POAG, including into the visual, working memory, attention and executive networks.[4–6,20–23] In addition, altered cerebral vascular autoregulation and vasoreactivity have been discovered in POAG patients.[24–29] To date, studies on cerebral blood perfusion in POAG have been mainly limited to the visual cortex, but the relationships between abnormal neurovascular activity and corresponding cerebral blood perfusion changes have not been elucidated. Evidence to date suggests that impairments in neurovascular coupling might contribute to the pathogenesis of POAG. Thus, we hypothesized that disturbed neurovascular coupling in visual and higher order cognitive cortices exists in patients with POAG and correlates with glaucoma stage and the severity of visual field defects.

Direct relationships among functional activity, metabolism, and blood flow have been demonstrated based on global measurements of cerebral metabolism and blood flow.[30] Brain regions with stronger connectivity tend to have higher spontaneous neuronal activity with greater metabolic demands, leading to increased perfusion.[30] The ratio of cerebral blood flow (CBF) to functional connectivity strength (FCS) measures the metabolic consumption per unit of connectivity strength, which reflects the relationship between the brain activity and perfusion, indirectly clueing on the neurovascular coupling of a specific voxel or local region. With this method, Liang et al.[31] found a tight coupling between blood supply and brain functional topology during resting state and its modulation in response to task demands. This new method has been successfully used in patients with schizophrenia,[32] Wilson's disease[33] and type 2 diabetes mellitus[34] to indirectly detect altered neurovascular coupling. To test our hypothesis that disturbed neurovascular coupling in visual and higher order cognitive cortices exists in patients with POAG and correlates with glaucoma stage and the severity of visual field defects, we investigate the altered CBF-FCS correlation coefficient and CBF/FCS ratio in the brain of patients with POAG, and we examined the correlations of the CBF/FCS ratio with clinical indices in patients with POAG.

Material and methods

This study was approved by the medical ethics committee of Beijing Tongren Hospital, and written informed consent in accordance with the Declaration of Helsinki was obtained from all participants. Forty-five POAG patients (22 males and 23 females, aged 43 ± 13.0 years) were recruited from the inpatient and outpatient clinics of our hospital, and comprised 12 early, 19 intermediate and 14 advanced-stage POAG patients. Twenty-five sex- and age-matched normal controls (NCs; 12 males and 13 females, aged 43 ± 10.6 years) were included in this study. All participants were righthanded. The demographics, clinical ophthalmic and neuropsychological assessments of all subjects are shown in the Table 1. The data sets of one patient and two NCs were excluded due to unqualified head movement, which affects image quality. Glaucoma was diagnosed according to the diagnostic criteria of the Primary Open-Angle Glaucoma Preferred Practice Pattern Guidelines of the American Academy of Ophthalmology.[35] These criteria include an open angle on gonioscopy and glaucomatous optic nerve head (ONH) and retinal nerve fiber layer (RNFL) changes, which are usually associated with typical glaucomatous visual field defects. All patients underwent a thorough history and physical examination including an ophthalmology examination. The inclusion criteria for the POAG patients were the following: (1) patient age between 30 and 65 years (2) a clinical examination confirming POAG, and (3) presence of both glaucomatous damage to the optic nerve and glaucomatous visual field defect. Three glaucoma specialists evaluated the examination results in a masked manner, and participants were enrolled in the study only when all three specialists agreed with the diagnosis. We excluded subjects with clinical evidence or history of other oculopathy; presence of significant psychiatric, neurological, or systemic comorbidity; detection of abnormal signals in the optic pathway or

Table 1. Clinical-demographic characteristics of the POAG and NC groups.

Clinical-demographic characteristics	POAG patients	NC	*P*
Age, mean ± SD (years)	43 ± 13.0	43 ± 10.6	0.862
Gender, male/female	22/23	12/13	0.943
MD, mean ± SD(dB)	−9.03 ± 6.40	−1.71 ± 1.56	<0.001
PSD, mean ± SD(dB)	6.44 ± 3.03	2.23 ± 1.31	<0.001
CDR, mean ± SD(μm)	0.68 ± 0.17	0.30 ± 0.09	<0.001
BDI	10.0 ± 8.8	3.6 ± 3.2	0.001
STAI-T	41.0 ± 9.7	32.5 ± 8.9	<0.001
STAI-S	39.0 ± 11.0	31.2 ± 9.2	0.003
MoCA	26.0 ± 3.3	26.0 ± 2.1	0.557
SDMT	53.0 ± 13.2	53.2 ± 10.4	0.957

MD: mean deviation; PSD: pattern standard deviation; CDR: cup-to-disc ratio; VF: visual field; STAI-S and STAI-T: state-trait anxiety inventory; BDI: Beck depression inventory; MoCA: Montreal cognitive assessment; SDMT: symbol digit modalities test.

brain on MRI (e.g. white matter hyperintensities, intracranial tumors, cerebral vascular lesions and previous cranial surgery); and contraindications to MRI scanning. NCs without clinical evidence or history of glaucoma were matched to the POAG patients in terms of age, sex and education.

Ophthalmologic examination and neuropsychological assessments

Each POAG subject underwent a comprehensive ophthalmologic examination, including visual acuity, refraction, slit-lamp biomicroscopy, applanation tonometry, gonioscopy, and dilated fundus examinations; optical coherence tomography (OCT); and visual field measurement. The mean deviation (MD) and pattern standard deviation (PSD) of the visual field defect were obtained after conducting a minimum of two standard automated perimetry examinations (central 30-2 full threshold program, Humphrey Field Analyzer; Zeiss Meditec AG, Jena, Germany) within a six-month period. To be considered reliable, a visual field had to meet the criteria of <20% fixation errors, <15% false positive results, and <33% false-negative results. Early-stage VF loss was defined as an MD higher than −6 dB; intermediate-stage visual field (VF) loss was defined as an MD between −12 and −6 dB, and advanced-stage VF loss was defined as an MD worse than −12 dB. The cup-to-disc ratio (CDR) was measured by spectral domain OCT (RTVue-100, software version 4.0; Optovue Inc., Fremont, CA).

A series of neuropsychological tests were administered to all patients to assess cognitive function (Montreal Cognitive Assessment, MoCA),[36] depression (Beck Depression Inventory, BDI),[37] anxiety (State-Trait Anxiety Inventory, STAI-T/S)[38] and information processing speed (Symbol Digit Modalities Test, SDMT).[39]

MRI data acquisition

Images were acquired on a 3.0-Tesla MR scanner (Discovery MR750; GE Healthcare, Milwaukee, WI, USA) using an 8-channel head coil. Structural 3D T1-weighted images were acquired with the following parameters: repetition time (TR) = 8.16 ms, echo time (TE) = 3.18 ms, inversion time (TI) = 450 ms, flip angle = 12°, matrix = 256 × 256, thickness = 1.0 mm, gap = 0 mm, slices =188 and voxel size = 1 × 1 × 1 mm^3. The rs-fMRI data were obtained using a gradient-echo single-shot echo planar imaging sequence with TE = 30 ms, TR = 2000 ms, slice thickness = 3 mm, gap = 1 mm, flip angle = 90°, FOV= 220 × 220 mm^2, matrix = 64 × 64, axial slices = 36 and time points = 180. The perfusion images were obtained using a pseudocontinuous ASL sequence with a 3D fast spin-echo acquisition and background suppression (TR = 5046 ms; TE = 10.5 ms; postlabel delay = 2025 ms; spiral in readout of 8 arms with 512 sample points; field of view- = 240 × 240 mm^2; reconstruction matrix =128 × 128; slice thickness = 3 mm, no gap; axial slices =50; number of excitation =3). CBF images were acquired from the raw ASL data by MRI scanner (Discovery MR750, GE Healthcare). The regional CBF is proportional to the difference in magnetization between control and tag conditions. The magnetization transfer effects of control and tag conditions were considered as equal for generating CBF images.

Before each scan, the subject was instructed to lie quietly with his or her eyes closed, relax, remain as still as possible, not think of anything in particular and not fall asleep. Foam padding and earplugs were used to limit head movement and attenuate scanner noise, respectively.

Rs-fMRI data preprocessing

The rs-fMRI data were preprocessed using DPABI (Yan et al.[40] provided in the public

domain, http://rfmri.org/DPABI) implemented in MATLAB (https://www.mathworks.com/products/matlab.html, MATLAB R2012a; The MathWorks, Inc., Natick, MA, USA). Data were converted to NIFTI format and the first 10 volumes were discarded. Slice timing and realignment for head motion correction for the remaining volumes were then performed. Subjects would be excluded due to head motion criteria (>1.5 mm translation or 1.5° rotation). Nuisance covariates were regressed out from the data, including signals of linear drift, six head movement parameters and their first-time derivations, and the signals of white matter, cerebrospinal fluid, and the whole brain. A temporal bandpass filter using a frequency range of 0.01–0.08 Hz was applied to the datasets. Each filtered functional volume was spatially normalized into standard Montreal Neurological Institute (MNI) space using nonlinear transformations and smoothed with a Gaussian smoothing kernel of 6-mm full-width at half-maximum (FWHM). Finally, the functional images were resampled into a 3-mm cubic voxel.

CBF analysis

CBF images were preprocessed using SPM12 software (SPM, www.fil.ion.ucl.ac.uk/spm) running on MATLAB (MATLAB R2012a; MathWorks, Inc., Natick, MA). The CBF maps were normalized to MNI space by the following steps: (1) The native CBF images were coregistered to structural 3D T1-weighted images of each subject. (2) The structural 3D T1-weighted images were spatially normalized to MNI space using the deformation fields generated during segmentation and normalization. (3) For each subject, the CBF image was written into the MNI space using the deformation parameter derived from the registration of T1-weighted images and was resliced into a 3-mm cubic voxel. The CBF maps were further standardized into z-scores using the following formula

$$\mathrm{zCBF}(i) = \frac{\mathrm{CBF}(i) - \mathrm{CBFgmean}}{\mathrm{CBFgstd}}$$

where zCBF(i) is the value at the i-th voxel on the z-score image of one subject, CBF(i) is the value at the i-th voxel on the CBF map, and CBFgmean and CBFgstd are the mean and STD, respectively, of the same subject within the gray matter region.[41]

Finally, each standardized CBF (zCBF) map was spatially smoothed with a 6-mm FWHM Gaussian kernel.

Whole gray matter FCS analysis

The whole gray matter FCS was calculated based on the following steps: first, a whole gray matter functional connectivity matrix for each participant was obtained by calculating Pearson's correlation coefficients between the BOLD time courses of all pairs of voxels within the gray matter (Nvoxels =67,541). Then, we computed the FCS using the following equation[42]

$$S_{\mathrm{voxel}}(i) = \frac{1}{N}\sum_{j \neq i} Z_{ij} \ r_{ij} > r_0$$

where r_{ij} is the correlation coefficient between voxel i and voxel j. r_0 was set to a threshold of 0.2 to eliminate weak correlations possibly arising from background noise,[32,42] and r_{ij} was converted to z_{ij} using Fisher's z-transformation when calculating FCS. Then, the z-maps of FCS were spatially smoothed with a 6-mm FWHM Gaussian kernel.

Relationship between FCS and CBF in whole gray matter

To quantitatively evaluate the relationship between FCS and CBF in whole gray matter, we performed correlation analyses across voxels for each subject.[31,32] Because the neighboring voxels could be highly dependent due to physiological correlations and spatial preprocessing, including registration and spatial smoothing, the effective degrees of freedom (*dfeff*) in across-voxel correlation analysis was much smaller than the number of voxels used in the analyses. When the voxel size ($v = 3 \times 3 \times 3$ mm^3) is much smaller than the spatial smoothness ("3dFWHMx" $= 6.550 \times 9.220 \times 9.776$ mm, estimated by DPABI), the spatial correlations are dominated by the spatial smoothing.[31] Thus, we need to consider the voxel-voxel dependence caused by spatial smoothing. The *dfeff* of across–voxel correlations was estimated based on the approximation formula by Liang et al.[31] in their CBF-FCS coupling study. The *dfeff* was then used to compute corrected P values in this study. Consequently, a CBF-FCS correlation coefficient within the whole gray matter was obtained for each participant. To explore the difference in CBF-FCS correlation coefficients between the POAG patients and NCs, a two-sample t test was performed.

Voxel-wise comparison analyses of the CBF/FCS ratio, CBF and FCS

To assess the regional coupling changes, we computed the CBF/FCS ratio (using the original CBF and FCS values without z-transformation) of each voxel. The CBF/FCS ratio of each voxel for each participant was transformed into a z-score to improve normality. Voxel-wise comparisons were then performed to investigate the intergroup difference in the CBF/FCS ratio using a two-sample t test with age and sex included

as nuisance variables. Subsequently, to further explore the early brain changes in POAG patients, we compared the CBF/FCS ratio via the voxel-wise analysis between early POAG patients and NCs. Multiple comparisons were corrected using a voxel-wise Gaussian random field (GRF) theory correction method with a voxel P value < 0.001, a voxel $Z > 3.09$ and a cluster P value < 0.05. For each participant, the mean CBF/FCS ratio of each cluster with significant group differences was extracted and used for the subsequent correlation analyses.

To better understand what may dominate the differences in the CBF/FCS ratio, we performed voxel-wise comparisons to identify CBF or FCS differences between the two groups while controlling for age and sex. Multiple comparisons were corrected using a voxel-wise GRF method (voxel $P < 0.001$, voxel $Z > 3.09$ and cluster $P < 0.05$).

Correlation analysis

Pearson correlation analyses were used to test the associations between the CBF/FCS ratio of each significantly changed cluster and both ophthalmologic measures (MD, PSD and CDR) and neuropsychological assessments (BDI, STAI-T/S, MoCA and SDMT score) of the POAG patients. The association between the glaucoma stage of patients and the CBF/FCS ratio was tested by nonparametric Spearman's rank correlation analysis. Multiple comparisons were corrected using the Bonferroni method ($P < 0.05/7 = 0.0071$).

Validation analyses

Given that gray matter volume (GMV) atrophy may affect CBF/FCS ratio changes, we analyzed intergroup differences in both GMV and density to evaluate whether any significant gray matter changes were evident in the POAG patient. We compared GMV between the POAG and NC groups using a two-sample t test in SPSS and applied a voxel-wise comparison to identify structures that differed significantly in volume between the two groups. Because gray matter atrophy has been reported previously in POAG patients, we repeated the voxel-wise CBF/FCS ratio comparisons with GMV as an additional covariate to exclude the effect of gray matter atrophy.

Results

Spatial distributions of FCS, CBF and the CBF/FCS ratio

The maps of the spatial distributions of FCS, CBF and the CBF/FCS ratio from the patients with POAG and NCs are shown in Figure 1(a). The distributions are similar between the two groups. Both groups showed higher values of CBF, FCS and the CBF/FCS ratios in the visual and auditory cortices, the default mode network (including the posterior cingulate cortex, precuneus and medial prefrontal cortex), the sensorimotor network (including the paracentral gyrus, comprising the precentral and postcentral gyri), and the superior and middle temporal gyri and temporal pole that comprise the attentional network.

CBF-FCS coupling changes within the whole gray matter of the POAG patients

Compared with the NCs, the POAG patients showed trend of lower global CBF (POAG: 50.15 ± 1.071 ml/100 g/min; NC: 53.15 ± 2.141 ml/100 g/min; two-sample t test, $t = -1.393$, $P = 0.1678$) and global FCS (POAG: 1.012 ± 0.001128; NC: 1.012 ± 0.001733; two-sample t test, $t = -0.1706$, $P = 0.8650$) in whole gray matter. Significant correlations between CBF and FCS were identified in all participants. Two representative correlation maps from one POAG patient and one NC are displayed in Figure 1(b); the POAG patients showed reduced CBF-FCS coupling compared with the NCs ($t = -2.901$, $P = 0.0049$) (Figure 1(c)).

CBF/FCS ratio changes in the POAG patients

Compared with the NCs, the POAG patients showed decreased CBF/FCS ratios in the bilateral lingual gyri extending to the calcarine gyri, bilateral rectal gyri, right superior and inferior temporal gyri, and left inferior frontal gyrus and an increased CBF/FCS ratios in the right angular and right middle frontal gyri (GRF correction voxel P value < 0.001 and cluster P value < 0.05, cluster size 18 voxels) (Figures 2 and 3(c) and Table 2). Reduced CBF/FCS ratio in the bilateral lingual gyri and increased CBF/FCS ratio in the right angular and middle frontal gyrus were detected in the early POAG patients (GRF-corrected voxel P value < 0.001 and cluster P value < 0.05) (Supplemental Figure S1, Supplemental Table S1).

CBF and FCS changes in the POAG patients

Compared with the NCs, the POAG patients exhibited decreased CBF in the bilateral lingual and calcarine gyri, right postcentral gyrus extending to right inferior frontal gyrus, supramarginal gyrus and inferior parietal lobule, left supramarginal gyrus, left inferior parietal lobule, and bilateral cerebellum and increased CBF in the bilateral rectal gyri, middle frontal gyri, right medial frontal gyrus, right superior frontal gyrus and right insula (GRF-corrected voxel P value < 0.001 and cluster P value < 0.05; cluster size: 31 voxels) (Figure 3(a)).

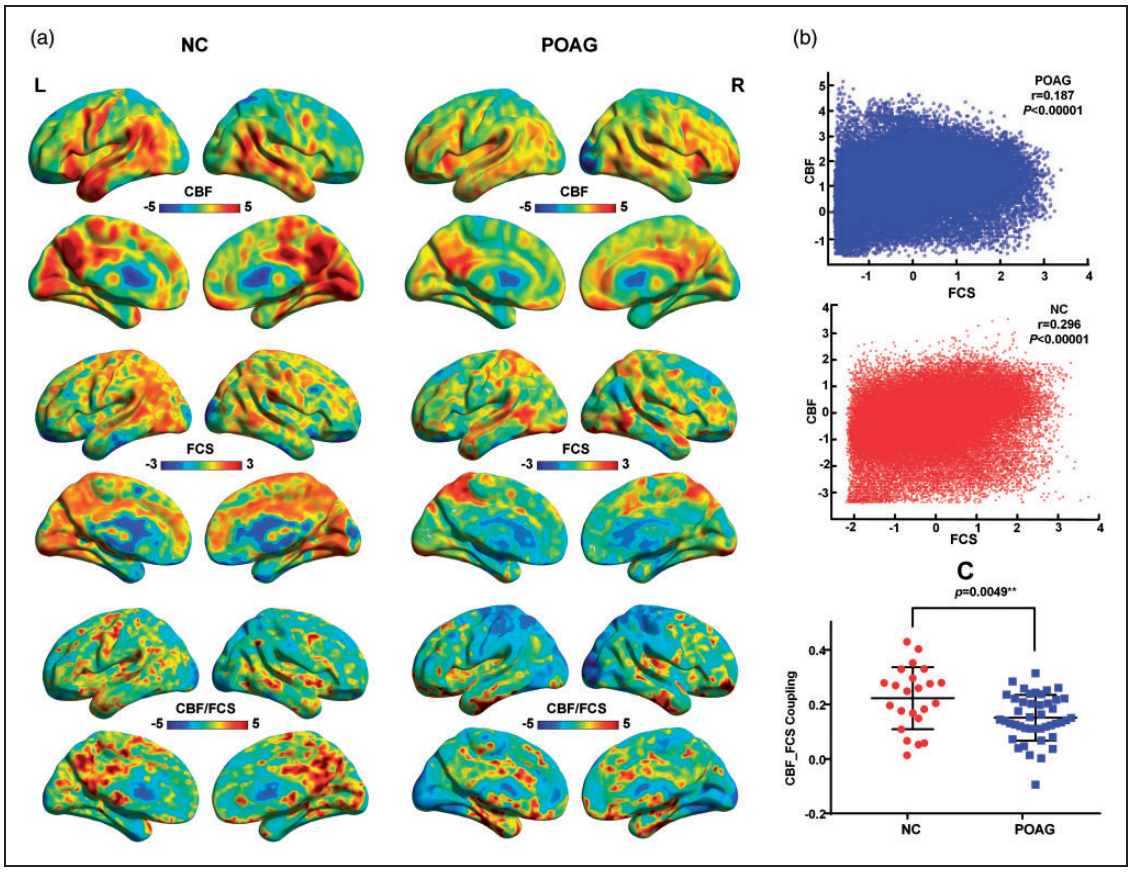

Figure 1. Spatial distribution maps and reduced neurovascular coupling in patients with POAG. (a) Examples of the mapped spatial distributions of FCS, CBF and the CBF/FCS ratio in a patient with POAG and an NC. The two subjects exhibited similar spatial distributions in these measures. (b) Scatter plots demonstrating the spatial correlations across voxels between CBF and FCS in the same subjects (blue, patient; red, NC) represented in Figure 1(a). (c) Compared with NCs, POAG patients showed reduced CBF-FCS coupling within gray matter ($P = 0.0049$). FCS: functional connectivity strength; CBF: cerebral blood flow; POAG: primary open-angle glaucoma.

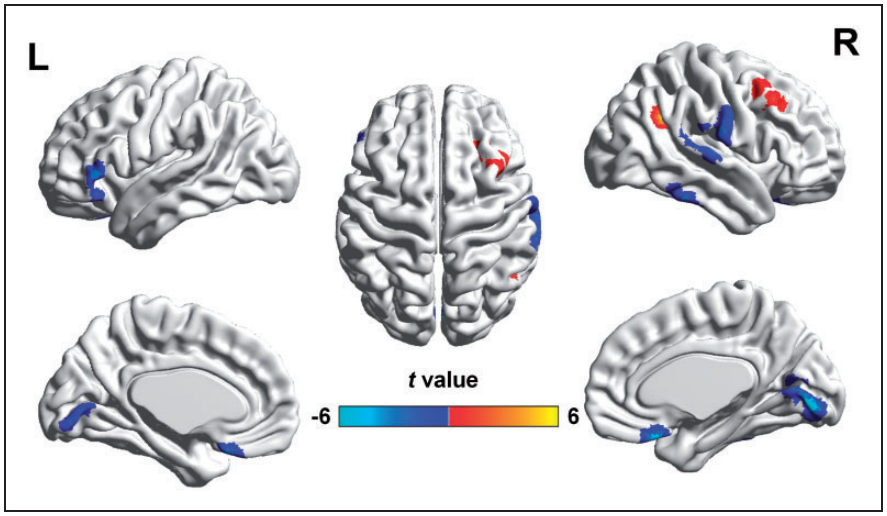

Figure 2. Altered CBF/FCS ratios in POAG patients compared with NCs (GRF-corrected voxel P value < 0.001 and cluster P value < 0.05). Compared with NCs, POAG patients exhibited decreased CBF/FCS ratios (cool colors) in the bilateral lingual gyri, bilateral rectal gyri, right superior and inferior temporal gyri, and left inferior frontal gyrus and increased CBF/FCS ratio (warm colors) in the right angular and right middle frontal gyri. FCS: functional connectivity strength; CBF: cerebral blood flow; POAG: primary open-angle glaucoma; GRF: Gaussian random field.

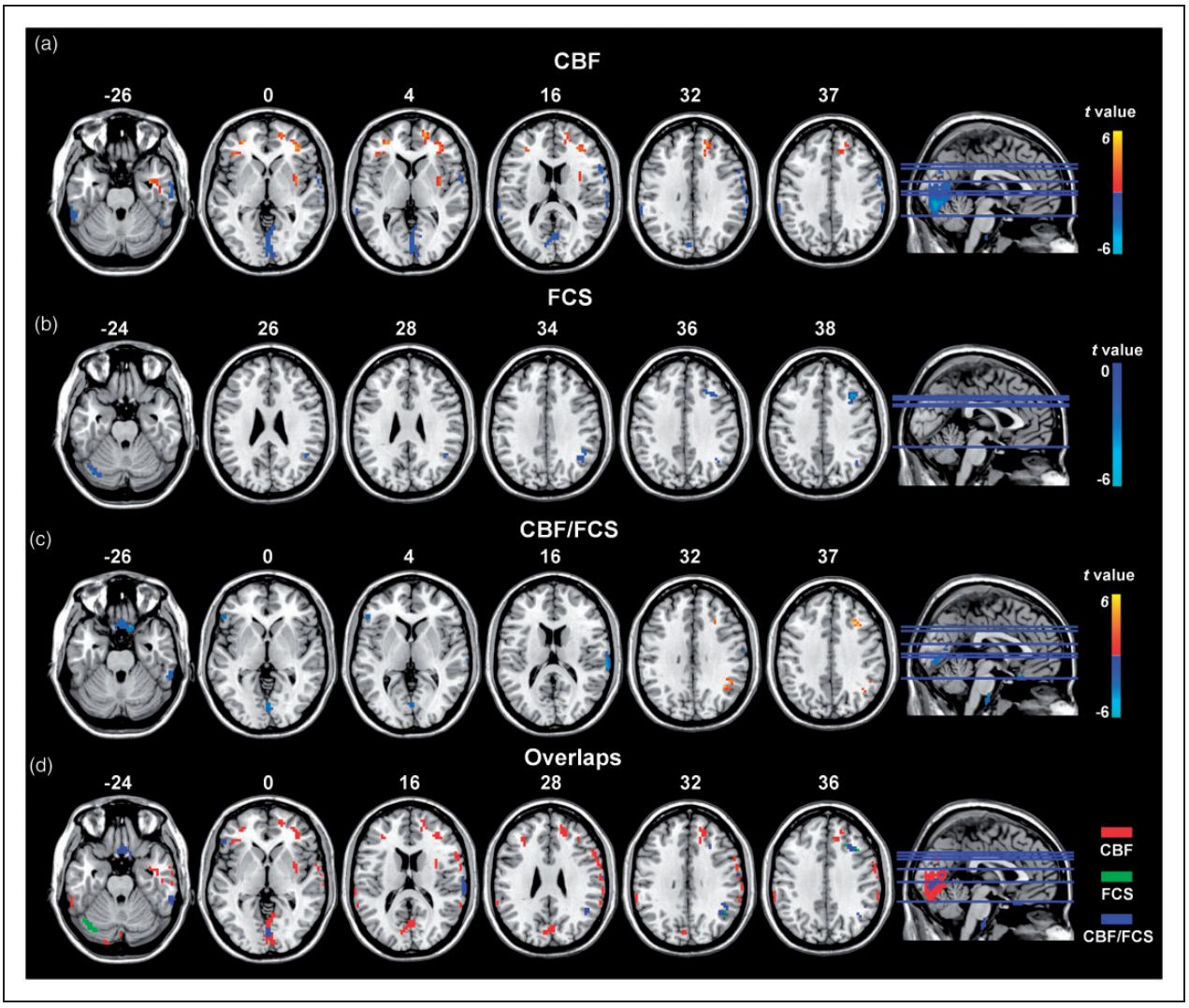

Figure 3. Altered CBF, FCS, and CBF/FCS ratio in POAG patients compared with NCs (GRF-corrected voxel P value < 0.001 and cluster P value < 0.05). (a) (b) and (c) show significantly increased (warm colors) and decreased (cool colors) CBF, FCS, and the CBF/FCS ratios, respectively, in patients with POAG. The regions in volume space (Figure 3(c)) are mapped into the surface space towards cortical vertex (Figure 2). (d) The overlay of clusters with significant differences between the two groups in CBF (red), FCS (green) and the CBF/FCS ratio (blue) indicated that the abnormal CBF/FCS ratios in POAG patients are predominantly driven by the CBF changes.

In addition, compared with NCs, the POAG patients showed decreased FCS in the right angular and middle frontal gyri and left cerebellum crus (GRF-corrected voxel P value < 0.001 and cluster P value < 0.05; cluster size: 22 voxels) (Figure 3(b)).

Correlation analysis of the CBF/FCS ratio and clinical indices

The correlations between the CBF/FCS ratio of each significant cluster and ophthalmologic measures and neuropsychological assessments of the POAG patients are shown in Table 3. In the POAG patients, the reduced CBF/FCS ratio was negatively correlated with glaucoma stage (Spearman's $\rho = -0.438$, $P = 0.004$) and positively correlated with MD ($r = 0.437$, $P = 0.004$) in the lingual gyrus (Supplemental Figure S2). While there was only a trend towards a negative correlation between the CBF/FCS ratio and CDR in the lingual gyrus ($r = -0.375$, $P = 0.017$), the significance did not remain after Bonferroni correction ($P < 0.05/7 = 0.0071$). We did not find significant correlations between the CBF/FCS ratio and any of the neuropsychological assessments values (Bonferroni correction, $P < 0.05/7 = 0.0071$).

Validation analyses

We found no significant difference in global GMV between POAG and NC groups ($GMV_{POAG} = (1.05 \pm 0.02) \times 10^6$ mm^3, $GMV_{NC} = (1.07 \pm 0.03) \times 10^6$ mm^3;

Table 2. Brain regions with significant differences in CBF/FCS ratios between POAG and NC groups.

Brain regions	Voxels	MNI coordinates(mm)			Peak intensity
		x	y	z	
POAG < NC					
Lingual gyrus	50	3	−84	−6	−4.8985
Rectal gyrus	47	0	21	−24	−4.8377
Left inferior frontal gyrus	18	−51	27	−9	−4.9389
Right inferior temporal gyrus	37	48	−42	−33	−4.8183
Right superior temporal gyrus	49	66	−30	15	−5.2981
POAG > NC					
Right angular	29	39	−54	33	4.3347
Right middle frontal gyrus	33	30	24	36	4.6411

Note: GRF correction voxel Z>3.090232, cluster $P < 0.05$, cluster size 18 voxels.
FCS: functional connectivity strength; CBF: cerebral blood flow; POAG: primary open angle glaucoma; NC: normal controls; GRF: Gaussian random field theory.

two-sample t test, $t = 0.595$, $P = 0.554$). There were no clusters survived after correction for multiple comparisons in voxel-based analysis between the two groups. Therefore, we used an "explorative" uncorrected threshold of $P < 0.001$ and clusters ≥ 100 voxels, and found visual cortex atrophy extending to the limbic lobe (cluster size: 552 voxels, peak MNI coordinates: X = 6, Y = −70.5, Z = 12; Supplemental Figure S3).

After correction with GMV as an additional covariate of no interest, the brain regions with altered CBF/FCS ratio showed similar distributions to those observed without GMV correction, although the cluster size was smaller (Figure 4 and Supplemental Table S2). The results suggested that most of the CBF/FCS ratio changes were independent of GMV atrophy in POAG.

Discussion

Consistent with our hypothesis, whole gray matter CBF-FCS coupling was lower in the POAG group than in the NC group, and voxel-wise whole brain analyses of the CBF/FCS ratio can provide more detailed information on the changes of brain functional regions. The brain regions with abnormal CBF/FCS ratios in the patients with POAG were components of the visual cortices, salience network, default mode network and dorsal attentional network, and included the lingual gyrus, angular, temporal and prefrontal regions. The reduced CBF/FCS ratio in the lingual gyrus was significantly correlated with the MD of visual field defects and glaucoma stage in the POAG patients, showing the clinical relevance this index. Moreover, reduced CBF/FCS ratio in the visual cortex and increased CBF/FCS ratio in the right angular and middle frontal gyrus were detected in patients with early POAG.

A significant across-voxel correlation between CBF and FCS was found in both the NCs and patients with schizophrenia in previous studies by Liang et al. and Zhu et al.,[31,32] providing clue on the neurovascular coupling in the physiology and pathology of the human brain. The CBF/FCS ratio maintains balance in healthy brains. The balance of the CBF/FCS ratio can be disrupted in POAG, with CBF and FCS changing in the opposite direction. For example, a subtle increase in CBF and decrease in FCS may result in a significantly increased CBF/FCS ratio in POAG, indicating redundant blood supply per unit of neuronal activity, whereas a subtle decrease in CBF and increase in FCS may result in a significantly decreased CBF/FCS ratio, suggesting an inadequate blood supply per unit of neuronal activity. Any single or combined impairment of the neurovascular unit components can lead to abnormal neurovascular coupling.[43]

Neurons and vessels are important components of the neurovascular unit. Neurons can transmit direct and indirect vasoactive signals for the appropriate delivery and distribution of CBF[44] and are thought to be the driving force behind neurovascular coupling due to their high energy demand. Changes in the GMV and neuronal activity within and beyond the visual system due to the neurodegenerative process in patients with POAG have been investigated in both histological and neuroimaging studies.[3,6,21,45] The observed cerebral volume reduction and neuronal loss or reorganization may contribute to the reduced neurovascular coupling in POAG. Various researchers have found vascular dysfunction in POAG patients, extending from the choroids,[46] optic nerve head,[12] central retinal artery,[47] and perifoveal macular capillaries[48] to the cerebral vasculature. Generalized abnormalities in the vascular endothelium appear to be representative of vascular dysregulation in POAG patients.[49]

Table 3. Correlations between CBF/FCS ratio and ophthalmic examination, and neuropsychological assessments.

Regions *t*-value (*P*-value)	MD	PSD	CDR	VF severity	STAI-S	STAI-T	BDI	MoCA	SDMT
Lingual gyrus	0.437 (0.004**)	−0.183 (0.259)	−0.375 (0.017*)	−0.438 (0.004)**	−0.179 (0.258)	−0.100 (0.529)	−0.142 (0.377)	0.325 (0.036)*	0.060 (0.740)
Rectal gyrus	0.250 (0.114)	−0.275 (0.086)	−0.275 (0.086)	−0.152 (0.342)	−0.001 (0.996)	0.001 (0.995)	0.110 (0.495)	0.044 (0.782)	−0.288 (0.104)
Left inferior frontal gyrus	0.085 (0.598)	−0.083 (0.611)	−0.274 (0.088)	−0.103 (0.521)	−0.069 (0.666)	0.105 (0.508)	0.068 (0.673)	0.107 (0.499)	−0.059 (0.746)
Right middle frontal gyrus	−0.115 (0.473)	0.156 (0.335)	0.136 (0.404)	0.255 (0.108)	0.092 (0.562)	−0.033 (0.838)	−0.300 (0.057)	−0.079 (0.620)	0.157 (0.383)
Right angular	0.180 (0.260)	−0.020 (0.904)	0.088 (0.587)	−0.115 (0.473)	−0.126 (0.428)	−0.243 (0.121)	−0.254 (0.108)	0.189 (0.230)	0.139 (0.441)
Right superior temporal gyrus	0.077 (0.631)	−0.072 (0.659)	−0.010 (0.953)	−0.108 (0.501)	0.134 (0.397)	0.154 (0.329)	0.097 (0.545)	0.069 (0.663)	−0.100 (0.579)
Right inferior temporal gyrus	0.087 (0.588)	−0.197 (0.223)	−0.032 (0.843)	−0.128 (0.423)	−0.161 (0.309)	−0.097 (0.542)	−0.005 (0.978)	0.041 (0.798)	−−0.190 (0.290)

MD: mean deviation; PSD: pattern standard deviation; CDR: cup-to-disc ratio; VF: visual field; STAI-S and STAI-T: state-trait anxiety inventory; BDI: Beck depression inventory; MoCA: Montreal cognitive assessment; SDMT: symbol digit modalities test.
*$p < 0.05$, **$p < 0.001$.

The POAG patients showed decreased CBF/FCS ratios in the bilateral lingual gyri, bilateral rectal gyri, right superior temporal gyrus, right inferior temporal gyrus and left inferior frontal gyrus. Reduced CBF and normal FCS were found in these regions in the POAG patients, suggesting that the decreased CBF/FCS ratios in these regions were predominantly driven by CBF decrease. Furthermore, the patients with POAG exhibited an increased CBF/FCS ratio in the right angular and right middle frontal gyri, which were mainly due to reductions in FCS. Decreased GMV, reduced low-frequency fluctuation (ALFF) and decreased FC in these brain regions have been reported in POAG patients.[6,22,50,51] The lingual gyrus of the occipital lobe is part of the primary visual cortex, and the inferior temporal gyrus is located in the ventral visual stream. The reductions in the CBF/FCS ratio in these regions suggest that in both the primary and higher visual cortices, trans-synaptic degeneration of the visual pathway and input reduction may be the main reasons for the dysfunction.[52] In line with previous studies, early brain changes were detected in the current study.[53,54] Moreover, CBF/FCS ratio in the lingual gyrus was significantly correlated with glaucoma stage and the MD of visual field defects in the POAG patients in our study. These results indicate altered CBF/FCS ratio might be a useful biomarker for investigating disease progression and pathologic changes in POAG.

The neurovascular unit is a central feature in the pathophysiology that leads to neurodegenerative disorders. In this study, several brain regions that exhibited significant changes in the CBF/FCS ratio or CBF are important for cognitive processing. The inferior frontal gyrus, medial frontal gyrus and insula are components of the salience network (SAL),[55,56] which accounts for executive control and working memory function, and may play important roles in neural reorganization following sensory deprivation. The rectal gyrus, angular gyrus and supramarginal gyrus are located in the default mode network (DMN).[55,56] The middle frontal gyrus and inferior parietal lobule are components of the dorsal attentional network (DAN),[57] which mediates attention, working memory and higher order cognitive processes. These changes were in accordance with previous studies suggesting neurodegenerative processing in POAG,[58] which might be related to the abnormalities in reading,[59] visual search,[60] face recognition,[61] visual object categorization,[62] dividing attention[59] and way finding observed in POAG patients. However, we did not find any significant correlations between the neuropsychological assessment indices and the CBF/FCS ratio. This lack of significant correlations may be because the abnormalities in the brain have not yet been demonstrated or because the scales

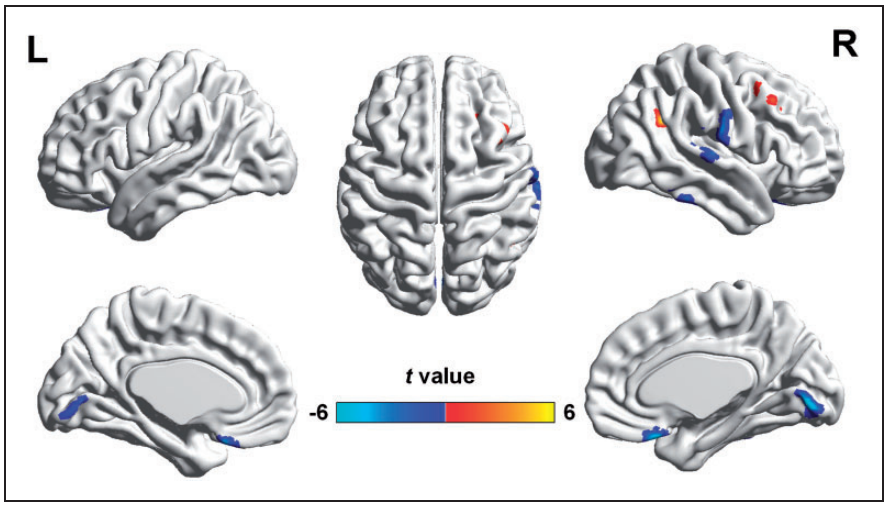

Figure 4. Altered CBF/FCS ratios in POAG patients compared with NCs after including GMV as a covariate (GRF-corrected voxel *P* value < 0.001 and cluster *P* value < 0.05). The warm and cool colors denote significantly increased and decreased CBF/FCS ratio, respectively, in POAG patients. CBF: cerebral blood flow; FCS: functional connectivity strength; GMV: gray matter volume; POAG: primary open-angle glaucoma; NCs: normal controls; GRF: Gaussian random field.

used were not sensitive enough. The underlying mechanisms should be investigated, and more sensitive and specific neuropsychological scales should be administered in future.

Astrocytes are another type of pivotal component of the neurovascular unit, controlling the extracellular environment for neurons and playing a fundamental role in regulating blood flow to the brain. Tamm and Dowling[17] reported that astrocytes were a critical element in glaucoma pathophysiology.[17] ONH astrocytes in patients with glaucoma were observed to have lower basal levels of antioxidant glutathione, which plays an important role in protecting the mitochondrial electron transport chain from damage by oxidative stress in both astrocytes and neurons. Furthermore, Yi et al.[63] investigated the responses of the lateral geniculate nucleus (LGN) to experimental glaucoma in monkeys and suggested that astrocytes may play an important role in the regulation of the LGN microenvironment in glaucoma. Lam et al.[18] demonstrated that robust astrocyte activation was evident in the LGN and V1 region of the visual cortex within the initial 60 days in a primate model of ocular hypertension (OHT) and that these changes were accompanied by early metabolic activity loss. Abnormal astrocytes can prevent normal interactions between neuronal activity and the vascular response, which is an important explanation for neurovascular decoupling.

Myo-inositol, as a marker of astrocytes, has been widely studied using proton magnetic resonance spectroscopy (1H-MRS); however, the results of MRS studies of patients with glaucoma are controversial and no consensus has yet been reached. Changes in myo-inositol have not been detected in glaucoma patients via MRS, although they have been found in other diseases. Myo-inositol and choline compounds are the predominant metabolites in glial cells, while N-acetylaspartate and glutamate have been reported at high concentrations in neurons. Due to the specific compartmentation of these metabolites in nervous tissue, MRS might not allow accurate metabolite quantification in specific cell cultures or samples of sorted cells under in vivo conditions.

Recent studies have confirmed that diffusion-weighted MRS (DW-MRS) can allow characterizations of specific metabolites (including myo-inositol) in vivo by quantifying diffusion properties, which depend on the cellular structure constraining them.[64] Ligneul et al.[65] successfully used DW-MRS to non-invasively monitor astrocytic structural alterations via specific variations of myo-inositol diffusion. However, few studies have evaluated metabolite diffusion in the human brain using 1H-MRS because the scan time required is too long to be tolerable to study participants. Although Hanstock and Beaulieu[66] proposed a new MRS methodology to obtain data quickly, their DW-MRS method nonetheless requires a 12-min acquisition time on a 4.7 T MRI. Although the new method, developed for use with 4.7 T scanners, has great potential for shortening the scanning time, it is currently impractical for most hospitals because most MRI scanners presently employed for clinical use are 3 T and 1.5 T scanners.

There are several limitations in the study. First, the number of participants was low, which limits the statistical power of the study; thus, the findings need to be

validated with a larger dataset. Second, subjects of young age were chosen to reduce the influence of any confounding effect of age on the functional MRI results, and we excluded seven subjects due to intracerebral lesions. These conditions may have introduced selection bias. Third, CBF-FCS correlations and CBF/FCS ratios are indirect measures of neurovascular coupling, and do not allow accurate evaluations of the neurovascular unit or determination of the pathophysiological mechanisms underlying the altered neurovascular coupling. Fourth, in this study, T2-flair was used to detect intracerebral ischemic lesions in subjects. Considering that vessel stenosis or occlusions can affect uniform spin labeling and thereby result in spurious loss of signal and changes in CBF, it would be useful to evaluate the vessel status of the cerebral artery via cerebrovascular imaging in the future. Fifth, we extracted clusters that showed significant changes for subsequent correlations analysis; this procedure may constitute a form of circular analysis and potentially inflated the significance of the results. Finally, although the POAG patients complained of abnormal important cognitive functions and although we detected abnormalities in the SAL, DMN and DAN, we did not determine whether these abnormalities were correlated with cognitive impairments. Specific task stimuli in fMRI and a series of more detailed neuropsychological assessments are needed to obtain further information in the future.

Conclusion

The patients with POAG showed disrupted coupling between resting-state CBF and functional connectivity. In addition, the CBF/FCS ratio in the lingual gyrus was decreased in these patients and was significantly correlated with the MD of visual field defects and glaucoma stage, emphasizing the clinical relevance of the CBF/FCS ratio. The abnormal CBF/FCS ratio in the higher order cognitive networks involving the SAL, DMN and DAN in the POAG patients implied that the detection of neurovascular decoupling in the brain may be informative for monitoring the disease progression and for understanding the pathophysiology of the neurodegenerative process in POAG.

Funding

The author(s) disclosed receipt of the following financial support for the research, authorship, and/or publication of this article: This study was supported by the National Natural Science Foundation of China under grants 81571649, 81901719, 81701666, and 81871340; Beijing Municipal Administration of Hospitals' Ascent Plan (DFL20190203); and Beijing Municipal Administration of Hospitals Clinical Medicine Development of Special Funding Support (ZYLX201704).

Acknowledgments

We acknowledge the participants of our study for their contribution and our team members for their support.

Declaration of conflicting interests

The author(s) declared no potential conflicts of interest with respect to the research, authorship, and/or publication of this article.

Authors' contributions

All authors contributed to the manuscript. Qian Wang designed and carried out the study, contributed to data analysis and drafted the manuscript. Xiaoxia Qu contributed to the study design, data analysis and interpretation and advised on the final drafting of the manuscript. Weiwei Chen and Huaizhou Wang contributed to subject recruitment for the study. Caiyun Huang contributed to data collection. Ting Li advised on data analysis. Ningli Wang and Junfang Xian contributed to the design of the research and advised on data analysis and final drafting of the manuscript.

Supplementary material

Supplemental material for this article is available online.

References

1. Jonas JB, Aung T, Bourne RR, et al. Glaucoma. *Lancet* 2017; 390: 2183–2193.
2. Tham YC, Li X, Wong TY, et al. Global prevalence of glaucoma and projections of glaucoma burden through 2040: a systematic review and meta-analysis. *Ophthalmology* 2014; 121: 2081–2090.
3. Kasi A, Faiq MA and Chan KC. In vivo imaging of structural, metabolic and functional brain changes in glaucoma. *Neural Regen Res* 2019; 14: 446–449.
4. Gracitelli CP, Duque-Chica GL, Sanches LG, et al. Structural analysis of glaucoma brain and its association with ocular parameters. *J Glaucoma* 2020; 29: 393–400.
5. Minosse S, Floris R, Nucci C, et al. Disruption of brain network organization in primary open angle glaucoma. *Conf Proc IEEE Eng Med Biol Soc* 2019; 2019: 4338–4341.
6. Wang Y, Wang X, Zhou J, et al. Brain morphological alterations of cerebral cortex and subcortical nuclei in high-tension glaucoma brain and its associations with intraocular pressure. *Neuroradiology* 2020; 62: 495–502.
7. Xu XH, Zou JY, Geng W, et al. Association between glaucoma and the risk of Alzheimer's disease: a systematic review of observational studies. *Acta Ophthalmol* 2019; 97: 665–671.
8. Gupta V, You Y, Li J, et al. BDNF impairment is associated with age-related changes in the inner retina and exacerbates experimental glaucoma. *Biochim Biophys Acta* 2014; 1842: 1567–1578.

9. Yoneda S, Hara H, Hirata A, et al. Vitreous fluid levels of beta-amyloid((1-42)) and tau in patients with retinal diseases. *Jpn J Ophthalmol* 2005; 49: 106–108.
10. Sharp PS, Ameen-Ali KE, Boorman L, et al. Neurovascular coupling preserved in a chronic mouse model of Alzheimer's disease: methodology is critical. *J Cereb Blood Flow Metab*. Epub ahead of print 23 November 2019. DOI: 10.1177/0271678X19890830.
11. Gugleta K, Fuchsjager-Mayrl G and Orgul S. Is neurovascular coupling of relevance in glaucoma? *Surv Ophthalmol* 2007; 52(Suppl 2): S139–143.
12. Prada D, Harris A, Guidoboni G, et al. Autoregulation and neurovascular coupling in the optic nerve head. *Surv Ophthalmol* 2016; 61: 164–186.
13. Rojas B, Gallego BI, Ramirez AI, et al. Microglia in mouse retina contralateral to experimental glaucoma exhibit multiple signs of activation in all retinal layers. *J Neuroinflammation* 2014; 11: 133.
14. Wang L, Cioffi GA, Cull G, et al. Immunohistologic evidence for retinal glial cell changes in human glaucoma. *Invest Ophthalmol Vis Sci* 2002; 43: 1088–1094.
15. Phillips AA, Chan FH, Zheng MM, et al. Neurovascular coupling in humans: physiology, methodological advances and clinical implications. *J Cereb Blood Flow Metab* 2016; 36: 647–664.
16. Zonta M, Angulo MC, Gobbo S, et al. Neuron-to-astrocyte signaling is central to the dynamic control of brain microcirculation. *Nat Neurosci* 2003; 6: 43–50.
17. Tamm ER and Dowling JE. Astrocytes and glaucomatous neurodegeneration. *Exp Eye Res* 2017; 157: 1–4.
18. Lam D, Jim J, To E, et al. Astrocyte and microglial activation in the lateral geniculate nucleus and visual cortex of glaucomatous and optic nerve transected primates. *Mol Vis* 2009; 15: 2217–2229.
19. London A, Benhar I and Schwartz M. The retina as a window to the brain-from eye research to CNS disorders. *Nat Rev Neurol* 2013; 9: 44–53.
20. Nuzzi R, Dallorto L and Rolle T. Changes of visual pathway and brain connectivity in glaucoma: a systematic review. *Front Neurosci* 2018; 12: 363.
21. Wang Q, Chen W, Wang H, et al. Reduced functional and anatomic interhemispheric homotopic connectivity in primary open-angle glaucoma: a combined resting state-fMRI and DTI study. *Invest Ophthalmol Vis Sci* 2018; 59: 1861–1868.
22. Trivedi V, Bang JW, Parra C, et al. Widespread brain reorganization perturbs visuomotor coordination in early glaucoma. *Sci Rep* 2019; 9: 14168.
23. Zhang Q, Shu Y, Li X, et al. Resting-state functional magnetic resonance study of primary open-angle glaucoma based on voxelwise brain network degree centrality. *Neurosci Lett* 2019; 712: 134500.
24. Zhang S, Xie Y, Yang J, et al. Reduced cerebrovascular reactivity in posterior cerebral arteries in patients with primary open-angle glaucoma. *Ophthalmology* 2013; 120: 2501–2507.
25. Wang Q, Chen W, Qu X, et al. Reduced cerebral blood flow in the visual cortex and its correlation with glaucomatous structural damage to the retina in patients with mild to moderate primary open-angle glaucoma. *J Glaucoma* 2018; 27: 816–822.
26. Findl O, Rainer G, Dallinger S, et al. Assessment of optic disk blood flow in patients with open-angle glaucoma. *Am J Ophthalmol* 2000; 130: 589–596.
27. Wang Y, Fawzi AA, Varma R, et al. Pilot study of optical coherence tomography measurement of retinal blood flow in retinal and optic nerve diseases. *Invest Ophthalmol Vis Sci* 2011; 52: 840–845.
28. Spaide RF. Measurable aspects of the retinal neurovascular unit in diabetes, glaucoma and controls. *Am J Ophthalmol* 2019; 207: 395–409.
29. Lavery WJ, Muir ER, Kiel JW, et al. Magnetic resonance imaging indicates decreased choroidal and retinal blood flow in the DBA/2J mouse model of glaucoma. *Invest Ophthalmol Vis Sci* 2012; 53: 560–564.
30. Kuschinsky W. Coupling of function, metabolism, and blood flow in the brain. *Neurosurg Rev* 1991; 14: 163–168.
31. Liang X, Zou Q, He Y, et al. Coupling of functional connectivity and regional cerebral blood flow reveals a physiological basis for network hubs of the human brain. *Proc Natl Acad Sci U S A* 2013; 110: 1929–1934.
32. Zhu J, Zhuo C, Xu L, et al. Altered coupling between resting-state cerebral blood flow and functional connectivity in schizophrenia. *Schizophr Bull* 2017; 43: 1363–1374.
33. Hu S, Wu H, Xu C, et al. Aberrant coupling between resting-state cerebral blood flow and functional connectivity in Wilson's Disease. *Front Neural Circuits* 2019; 13: 25.
34. Hu B, Yan LF, Sun Q, et al. Disturbed neurovascular coupling in type 2 diabetes mellitus patients: evidence from a comprehensive fMRI analysis. *Neuroimage Clin* 2019; 22: 101802.
35. Prum BE, Jr., Rosenberg LF, Gedde SJ, et al. Primary open-angle glaucoma preferred practice pattern((R)) guidelines. *Ophthalmology* 2016; 123: P41–P111.
36. Nasreddine ZS, Phillips NA, Bedirian V, et al. The Montreal Cognitive Assessment, MoCA: a brief screening tool for mild cognitive impairment. *J Am Geriatr Soc* 2005; 53: 695–699.
37. Beck AT, Ward CH, Mendelson M, et al. An inventory for measuring depression. *Arch Gen Psychiatry* 1961; 4: 561–571.
38. Loo R. The state-trait anxiety inventory a-trait scale: dimensions and their generalization. *J Pers Assess* 1979; 43: 50–53.
39. Pascoe M, Alamri Y, Dalrymple-Alford J, et al. The symbol-digit modalities test in mild cognitive impairment: evidence from Parkinson's disease patients. *Eur Neurol* 2018; 79: 206–210.
40. Yan CG, Wang XD, Zuo XN, et al. DPABI: data processing & analysis for (resting-state) brain imaging. *Neuroinformatics* 2016; 14: 339–351.
41. Liu F, Zhuo C and Yu C. Altered cerebral blood flow covariance network in Schizophrenia. *Front Neurosci* 2016; 10: 308.
42. Wang L, Dai Z, Peng H, et al. Overlapping and segregated resting-state functional connectivity in patients

with major depressive disorder with and without childhood neglect. *Hum Brain Mapp* 2014; 35: 1154–1166.
43. Zlokovic BV. Neurodegeneration and the neurovascular unit. *Nat Med* 2010; 16: 1370–1371.
44. Attwell D, Buchan AM, Charpak S, et al. Glial and neuronal control of brain blood flow. *Nature* 2010; 468: 232–243.
45. Yucel YH, Zhang Q, Gupta N, et al. Loss of neurons in magnocellular and parvocellular layers of the lateral geniculate nucleus in glaucoma. *Arch Ophthalmol* 2000; 118: 378–384.
46. Ulrich A, Ulrich C, Barth T, et al. Detection of disturbed autoregulation of the peripapillary choroid in primary open angle glaucoma. *Ophthalmic Surg Lasers* 1996; 27: 746–757.
47. Galambos P, Vafiadis J, Vilchez SE, et al. Compromised autoregulatory control of ocular hemodynamics in glaucoma patients after postural change. *Ophthalmology* 2006; 113: 1832–1836.
48. Grunwald JE, Riva CE, Stone RA, et al. Retinal autoregulation in open-angle glaucoma. *Ophthalmology* 1984; 91: 1690–1694.
49. Su WW, Cheng ST, Ho WJ, et al. Glaucoma is associated with peripheral vascular endothelial dysfunction. *Ophthalmology* 2008; 115: 1173–1178.e1171.
50. Li T, Liu Z, Li J, et al. Altered amplitude of low-frequency fluctuation in primary open-angle glaucoma: a resting-state FMRI study. *Invest Ophthalmol Vis Sci* 2014; 56: 322–329.
51. Frezzotti P, Giorgio A, Toto F, et al. Early changes of brain connectivity in primary open angle glaucoma. *Hum Brain Mapp* 2016; 37: 4581–4596.
52. Lawlor M, Danesh-Meyer H, Levin LA, et al. Glaucoma and the brain: trans-synaptic degeneration, structural change, and implications for neuroprotection. *Surv Ophthalmol* 2018; 63: 296–306.
53. Wang R, Tang Z, Sun X, et al. White matter abnormalities and correlation with severity in normal tension glaucoma: a whole brain atlas-based diffusion tensor study. *Invest Ophthalmol Vis Sci* 2018; 59: 1313–1322.
54. Murphy MC, Conner IP, Teng CY, et al. Retinal structures and visual cortex activity are impaired prior to clinical vision loss in glaucoma. *Sci Rep* 2016; 6: 31464.
55. Espinoza FA, Anderson NE, Vergara VM, et al. Resting-state fMRI dynamic functional network connectivity and associations with psychopathy traits. *Neuroimage Clin* 2019; 24: 101970.
56. Wang D, Qin W, Liu Y, et al. Altered resting-state network connectivity in congenital blind. *Hum Brain Mapp* 2014; 35: 2573–2581.
57. Corbetta M and Shulman GL. Control of goal-directed and stimulus-driven attention in the brain. *Nat Rev Neurosci* 2002; 3: 201–215.
58. Frezzotti P, Giorgio A, Motolese I, et al. Structural and functional brain changes beyond visual system in patients with advanced glaucoma. *PLoS One* 2014; 9: e105931.
59. Swenor BK, Varadaraj V, Dave P, et al. Impact of the ability to divide attention on reading performance in glaucoma. *Invest Ophthalmol Vis Sci* 2017; 58: 2456–2462.
60. Smith ND, Glen FC and Crabb DP. Eye movements during visual search in patients with glaucoma. *BMC Ophthalmol* 2012; 12: 45.
61. Glen FC, Crabb DP, Smith ND, et al. Do patients with glaucoma have difficulty recognizing faces? *Invest Ophthalmol Vis Sci* 2012; 53: 3629–3637.
62. Lenoble Q, Lek JJ and McKendrick AM. Visual object categorisation in people with glaucoma. *Br J Ophthalmol* 2016; 100: 1585–1590.
63. Dai Y, Sun X, Yu X, et al. Astrocytic responses in the lateral geniculate nucleus of monkeys with experimental glaucoma. *Vet Ophthalmol* 2012; 15: 23–30.
64. Palombo M, Shemesh N, Ronen I, et al. Insights into brain microstructure from in vivo DW-MRS. *Neuroimage* 2018; 182: 97–116.
65. Ligneul C, Palombo M, Hernandez-Garzon E, et al. Diffusion-weighted magnetic resonance spectroscopy enables cell-specific monitoring of astrocyte reactivity in vivo. *Neuroimage* 2019; 191: 457–469.
66. Hanstock C and Beaulieu C. Rapid acquisition diffusion MR spectroscopy of metabolites in human brain. *NMR Biomed* 2020; e4270. DOI: 10.1002/nbm.4329.